Dynamic Shearing Resistance of Molten Metal Films Under High Pressures and Extremely High Shearing Rates

by Makoto Okada, Nai-Shang Liou, and Vikas Prakash

ABSTRACT—In the present study plate-impact pressure-shear experiments have been conducted to study the dynamic shearing resistance of molten metal films at shearing rates of approximately $10^7 s^{-1}$. These molten films are generated by pressure-shear impact of relatively low melt-point metals such as 7075-T6 Al alloy with high hardness and high flow-strength tool-steel plates. By employing high impact speeds and relatively smooth impacting surfaces, normal interfacial pressures ranging from 1–3 GPa and slip speeds of over 100 m/s are generated during the pressure-shear loading. The resulting friction stress (~100 to 400 MPa) combined with the high slip speeds generate conditions conducive to interfacial temperatures approaching the fully melt temperature regime of the lower melt-point metal (7075-T6 aluminum alloy) comprising the tribo-pair.

During pressure-shear loading, laser interferometry is employed to measure normal and transverse motion at the rear surface of the target plate. The normal component of the particle velocity provides the interfacial normal traction while the transverse component provides the shearing resistance of the interface as it passes through melt. In order to extract the critical interfacial parameters, such as the interfacial slip-speed and interfacial temperatures, a Lagrangian finite-element code is developed. The computational procedure accounts for dynamic effects, heat conduction, contact with friction, and full thermo-mechanical coupling. At temperatures below melt the flyer and target materials are described as an isotropic thermally softening elastic-viscoplastic solid. For material elements with temperatures in excess of the melt point, a purely Newtonian fluid constitutive model is employed. The results of this hybrid experimental-computational study provide insights into the dynamic shearing resistance of molten metal films at high pressures and extremely high shearing rates.

KEY WORDS—High speed sliding, dynamic confined molten metal films, high pressures, ultra-high strain rates, plate impact experiments

Introduction

The plastic flow of metals at high strains and high strain rates, studied extensively for nearly fifty years, has recently attracted renewed interest because of the discovery of strong effects at very high strain rates and elevated temperatures, and because of the growing acceptance of the importance of these effects in dynamic failure mechanisms.[1–4] Early interest in the subject was stimulated by military applications, especially armor penetration. While these applications continue to spur interest, the need to understand dynamic plastic flow under extreme conditions has been recognized as being of critical importance in a broad range of applications, including high-rate forming, high-speed machining, friction and explosive welding, and a variety of safety-related applications, ranging from the crash-worthiness of vehicles to the retention of flying pieces of broken turbine blades.

In an attempt to understand the high strain-rate behavior of materials, Kolsky[5] pioneered an experimental approach by which the response of materials under nominally homogeneous states of stress was measured by placing a short specimen between two elastic bars and using elastic waves in bars to impose the loading and monitor the nominal stress and strain in the specimen. With this approach, dynamic stress-strain curves at constant strain rates and elevated temperatures have been obtained for many metals at strain rates of 10^2 to 10^3 s^{-1}.[6,7] The basic concepts of the Kolsky approach have been extended to torsional loading by Duffy, Cambell and Hawley[8] and to tensile loading by Harding, Wood and Cambell,[9] Hauser,[10] Lindholm and Yeakley,[11] and Nicholas.[12]

In order to obtain the dynamic plastic response of the materials at higher levels of plastic strain-rates, normal and pressure-shear plate-impact experiments have been employed[13] in the past. Large strain rates have been obtained by reducing the thickness of the specimen to the thicknesses of, say, 200 to 50 μm. In this way, the flow stresses of pure metals (Al, Cu, Fe) have been shown to increase strongly with increasing strain rate at strain rates approaching $10^5 s^{-1}$ and higher.[14] Recently, Frutschy and Clifton[15] have extended pressure-shear plate impact experiments to investigate the dynamic shear strength of OFHC copper over temperature ranges from 300 to 700°C and strain rates from 10^5 to $10^6 s^{-1}$.

In an attempt to investigate the dynamic response of metals under high shearing rates and temperatures approaching melt, plate-impact type experiments have been conducted, in which specimens were made to enter the melt regime at moderate pressures by impacting a porous specimen. However, the material parameters inferred from these experiments were rather insensitive to whether melting actually occurred.[16]

Makoto Okada and Nai-Shang Liou are Graduate Students, and Vikas Prakash is an Associate Professor, Department of Mechanical and Aerospace Engineering, Case Western Reserve University, Cleveland, OH 44106-7222, USA.

Original manuscript submitted: October 23, 2000.
Final manuscript received: December 6, 2001.

In experiments conducted by Schmidt, *et al.*[17] significant strength effects were observed well into the melt regime for several metal alloys. Holsapple and Schmidt[18] employed electron-beam irradiation to heat metals into the melt regime. In these experiments, aluminum specimens heated to various initial temperatures by carbon-foil radiation heater, were exposed to high-energy electron beam radiation to push them into the fully-melt regime. Moreover, Schmidt[19] conducted plate impact experiments to investigate the strength of tungsten at near-melt conditions. In this series of experiments, heating and testing of the specimen was accomplished within a short period of time (<5 ms) using a capacitor discharge current coupled through a pulse transformer. The specimen itself was used as the heating element and was an integral part of the secondary circuit of the pulse transformer used to transfer energy from the capacitor bank to the specimen.

More recently, Mineev and Mineev[20] have determined the viscosity of molten aluminum and lead at strain rates in excess of $10^6 s^{-1}$, dynamic compressions above 2, normal pressures in the range of 35–250 GPa and temperatures in the 20000K range. The estimates of viscosity were made by studying the propagation of small perturbations in the shock-wave front through the molten metal. They concluded that, within the experimental errors of their setup and analysis, molten lead and aluminum could be modeled as a purely Newtonian fluid with a viscosity of approximately $2-4\times10^3$ Pa-s and nearly independent of the applied shearing strain rate.

The purpose of this paper is to present a novel experimental methodology to investigate the dynamic shearing resistance of metals as they pass through melt under large hydrostatic pressures and ultra-high shearing rates. These experiments are motivated by recent advances in experimental methods to investigate dynamic friction at high interfacial pressures, high slip-speeds and elevated temperatures.[21–25] The molten films are generated by plate-impact pressure-shear loading of relatively low melt-point metals, such as 7075-T6 Al alloy, with high hardness and high flow strength tool-steel plates. By employing relatively large impact speeds, and flyer and target plates with smooth impacting surfaces, normal interfacial pressures ranging from 1–3 GPa and interfacial slip speeds of over 100 m/s are generated. The resulting friction stress (100 to 400 MPa), combined with the relatively high slip-speeds, generate conditions conducive to interfacial temperatures approaching the near-melt and fully-melt regime of the lower melt-point metal (7075-T6 aluminum alloy) comprising the impacting material pair. During the pressure-shear loading laser interferometry is employed to measure both normal and transverse motion of the rear surface of the target plate. The normal component of the particle velocity provides the normal traction while the transverse component provides the evolution of the dynamic shearing resistance as the interface passes through melt. Moreover, in order to interpret critical interfacial parameters such as interfacial slip speed and temperatures, a Lagrangian finite element code is developed. The computational procedure accounts for dynamic effects, heat conduction, contact with friction, and full thermo-mechanical coupling. At temperatures below the melt regime the material is described as an isotropic thermally softening elastic-viscoplastic solid. For material elements with temperatures in excess of the melt point a purely Newtonian fluid constitutive model is employed.

In Section 2 the pressure-shear plate-impact experimental configuration used in the experiments is described. Section 3 provides details of wave propagation in the flyer and target plates. Section 4 gives the theoretical background useful for calculating the interfacial tractions, slip velocity and the interfacial temperatures. In Section 5 details about the finite element procedure used for simulating the experiments are provided. Section 6 describes the experimental results and discussion.

Plate-impact Pressure-shear Experiment

Experimental Configuration

The schematic of the plate impact pressure shear experimental configuration is shown in Fig. 1. The experiment involves the impact of a flyer plate mounted on a projectile with a stationary target plate. The flyer plate is fabricated from 7075-T6 Al alloy while the target is machined from Carpenter Hampden (AISI type D3) tool-steel (flow strength ~1800 MPa and T_{melt} ~1500°C). The choice of Al alloy for the flyer plate is dictated by its relatively low melt temperature, and is expected to be driven into its fully-melt temperature regime under the pressure-shear frictional loading. On the other hand, the choice for the D3 tool-steel as the target plate is driven by its high hardness and is expected to remain elastic during the pressure-shear impact.

Impact takes place in a vacuum, and prior to impact the impacting plates are aligned parallel to each other at an angle θ ~35° relative to the direction of approach. This results in combined pressure-shear loading at the flyer-target interface. The impact faces of the specimen and the target are lapped and polished to $R_a < 0.1$ μm. The use of relatively large skew-angle, together with smooth impact surfaces, is expected to promote high interfacial slip-speeds at the flyer/target interface. The condition that the target plate remains elastic during impact restricts the impact speeds to approximately 225 m/s (σ_n ~2 to 3 GPa). The combination of high slip-speeds and high interfacial normal pressure aids in elevating the temperature of the impacting surface of the Al alloy flyer plate to the point when the elevated temperature dynamic shearing resistance of the Al alloy is lower than the frictional resistance required for interfacial slip. When this condition is attained frictional slip ceases and a thin layer of molten Al alloy is sheared at high normal pressures and ultra-high shear strain rates.

During the experiment the velocity of the projectile and the history of normal and transverse particle velocities at the rear surface of the target plate are measured by laser interferometry. These measurements are used to infer the normal and shear tractions at the flyer-target interface. All measurements of the particle velocity are made before the arrival of

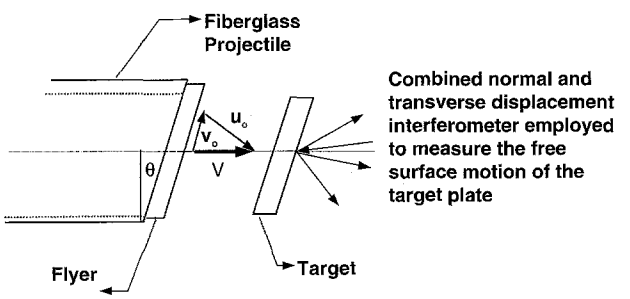

Fig. 1—Schematic of the plate impact pressure-shear experiment

the unloading waves from the lateral boundary of the specimen. In the view of this, and during the time interval of interest, the tribo-pair plates can be considered to be essentially infinite in their spatial dimensions and can be modeled as one semi-infinite half-plane sliding on the other. This simplification of the tribo-pair geometry allows one-dimensional elastic-plastic wave theory to be used in the interpretation of the experimental results.

A 82.5 mm (3.25") bore single-stage gas-gun at Case Western Reserve University is used to conduct the plate impact pressure-shear friction experiments. Using this gas gun, a fiberglass projectile, which carries the flyer plate, is accelerated down the gas barrel by means of compressed nitrogen gas. The rear end of the projectile has sealing O-ring and a plastic (Teflon) key that slides in a key-way inside the gun barrel to prevent any rotation of the projectile. The impact takes place in a target chamber that has been evacuated to 50 μm of Hg to reduce the air cushion between the flyer and the target plates at the impact. A laser based optical system utilizing a UNIPHASE Helium-Neon 5 mW laser (Model 1125p) and a high frequency photo-diode is used to measure the velocity of the projectile. To ensure the generation of plane waves with wave-front sufficiently parallel to the impact face, the flyer and the target plates are aligned to be parallel to within 2×10^{-5} radians by using an optical alignment scheme developed by Kim, Kumar and Clifton.[26] The actual tilt between the two plates is measured by recording the times at which four, isolated, voltage-biased pins, that are flush with the surface of the target plate, are shorted to ground. The acceptance level of the experiments is of the order of 0.5 mrad.[27]

A combined normal displacement (NDI) and transverse displacement (TDI) laser interferometer is used to measure the combined normal and transverse particle velocities at the rear surface of the target plate. COHERENT Innova 90 argon-ion laser with wavelength of 514.5 nm is used to provide the coherent monochromatic light source. The NDI[28] monitors the normal displacement of the rear surface of the target plate by combining a reference beam and a beam reflected from the target such that one peak to peak variation of the intensity of the light corresponds to a displacement of $\lambda/2$ (~0.25725 μm), where λ is the wavelength of the laser light in use. The TDI[26] monitors two nth order beams diffracted from a grating deposited on the rear surface of the target plate in order to get the phase difference between them. The TDI sensitivity is given by $\Delta v = d/2n$ (in our case, $\Delta v = 0.833$ μm/lines), where d is the pitch of the diffraction grating ($d = 1/D$), and D is the grating lines per mm in use (in our case, $D = 600$ lines/mm), and n is the order of the diffracted beams in use (in our case, $n = 1$). The interferometric signals from NDI and TDI are detected by NEWPORT Silicon PIN Detectors (model 818-BB-21) having a rise time of less than 1 ns. The output of the photo detectors is amplified and recorded on the high-speed digital oscilloscope (HEWLETT PACKARD 54542A oscilloscope, 2 GSa/s, 500 MHz). A digital data processing program is used to process the interferometric signals and calculate the history of the normal and transverse particle velocities at the rear surface of the target plate.

Flyer and Target Materials and Specimen Preparation

The physical properties of CH tool-steel and the 7075-T6 Al alloy are provided in Table 1. The dimensions of the CH tool-steel disk were 76 mm diameter and 9.5 mm thickness. The dimensions of the 7075-T6 Al alloy plate were 76.2 mm diameter and 20 mm thickness. Prior to the experiment, both sides of the flyer and the target plates are ground flat by using a surface grinder. The target and flyer plates are lapped flat on both sides to within 2-3 Newton's rings over the diameter. Lapping is performed on a Lapmaster machine using 14.5 μm aluminum oxide powder in mineral oil. A Hommel® T500 diamond stylus surface profile measurement device is used to determine the surface roughness profiles for the flyer and the target plates. To obtain the desired surface roughness, both the flyer and the target plates are polished on Texmeth cloth using 3 μm diamond paste. This procedure allows control of the surface roughness of the CH tool-steel plate between $R_q = 0.01$ and 0.02 μm (root-mean-square profile height, RMS), and that of the aluminum alloy 7075-T6 plate between $R_q = 0.07$ and 0.12 μm (RMS) without losing flatness.

Four copper pins, isolated electrically from the target, are placed in slots near the periphery of the impact face of the target plate. The first contact of any one of these pins with the flyer provides the triggering signal for the recording system. In addition, these pins are used to determine any *tilt* between the flyer and the target plates at impact. In order to measure the combined normal and transverse particle displacement history at the rear-surface of the target plate, a holographic diffraction grating of approximately 600 lines/mm is used.

Wave Propagation in the Target and Flyer Plates

The wave propagation in the flyer and the target plates is illustrated schematically as a time-distance diagram in Fig. 2. The figure represents the spatial position of the wave-front at a particular time. The solid lines represent the longitudinal wave fronts and the dashed line represents the shear wave front. The slope of the solid line represents the inverse of the longitudinal wave speed (C_L) while the slope of the dashed line represents the inverse of the shear wave speed (C_S). When the flyer plate impacts the target plate (point A on the time-distance diagram), both longitudinal and shear waves are generated in the flyer and the target plates. Thus, at impact, the flyer-target interface is at a compressive stress, σ_1, and a shear stress τ_1, which represents the frictional resistance of the flyer-target interface. For the 7075-T6 Al/CH tool-steel flyer-target combination employed in the present experiments the duration of the pressure-shear loading before the arrival of the release waves from the specimen boundary is approximately 2.8 μs.

Wave-analysis of Pressure-shear Friction Experiments: Calculation of Interfacial Tractions, Slip Velocity and Slip Distance

Let the projectile velocity at impact be denoted by V. Then, the initial normal and the transverse particle velocities of the flyer plate, u_o and v_o, respectively, can be expressed in terms of the skew angle θ and the impact velocity as

$$u_o = V\cos\theta \text{ and } v_o = V\sin\theta. \quad (1)$$

When the flyer impacts the target, both the normal and the transverse components of particle velocity are imposed on the impact face of the target plate. Using one-dimensional stress-wave analysis of the governing hyperbolic partial differential

TABLE 1—MATERIAL PROPERTIES OF THE TRIBO-PAIR MATERIALS

	FLYER Material Aluminum Alloy 7075-T6	TARGET Material Carpenter Hampden Steel
Longitudinal Wave Speed C_L, mm/μs	6.23	5.98
Transverse Wave Speed C_S, mm/μs	3.100	3.264
Acoustic Impedance ρC_L, GPa/mm/μs	17.44	45.50
Shear Impedance ρC_S, GPa/mm/μs	8.68	24.90
Mass Density ρ, kg/m	2800	7612
Young's Modulus E, GPa	71	207
Shear Modulus μ, GPa	26.9	81.1
Tensile Strength σ, MPa	572	2758
Thermal Conductivity k, W/mK	130	42.3
Thermal Diffusivity γ, m^2/s	48.4×10^6	12.2×10^{-6}
Specific Heat C_p, J/kg.K	960	422
Melt Temperature °C	635	1400

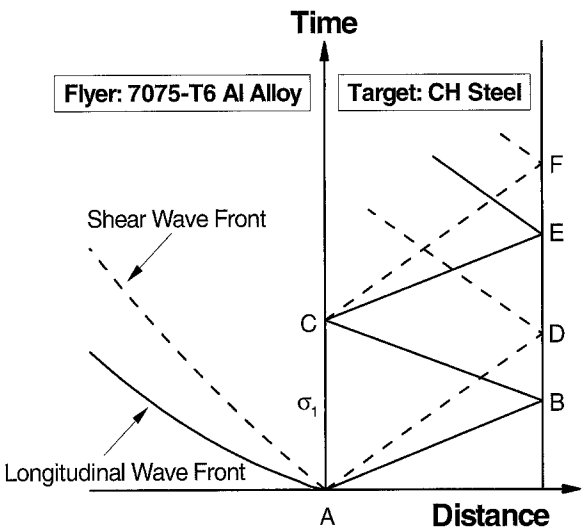

Fig. 2—Time-distance diagram for the pressure-shear friction experiment showing wave propagation in the target and flyer plates

equations, the normal and the shear tractions at the flyer-target interface can be expressed in terms of the measured normal and transverse particle velocities, $u_{fs}(t)$ and $v_{fs}(t)$, respectively, as

$$\sigma_1(t) = -\frac{(\rho C_L)_t}{2} u_{1fs}(t) \tag{2}$$

$$\tau_1(t) = \frac{(\rho C_S)_t}{2} v_{1fs}(t) \tag{3}$$

As mentioned earlier, in the present experiments the 7075-T6 Al alloy undergoes elastic-plastic deformation. As long as the impact speeds are restricted such that the CH tool-steel plate remains elastic during impact the normal and transverse components of the interfacial traction can be obtained by employing eqs (2) and (3). However, in order to obtain the interfacial slip speeds, and hence the frictional power, a full elastic-plastic finite-element simulation of the experiment is required.

This can be better understood from the shear-stress versus particle velocity diagram shown in Fig. 3, for the case of impact between an elastic-plastic flyer plate and an elastic target plate. The solid straight line passing through the origin represents the loci of all possible stress and particle velocity states that can be achieved on the target side of the frictional interface. However, the corresponding curve for the flyer side is replaced by a curve corresponding to the elastic-plastic response of the 7075-T6 Al flyer-plate. The interfacial slip-speed is given by the difference of the transverse particle velocities on either side of the frictional interface, i.e., $V_{slip}(t) = V_B(t) - V_C(t)$. The transverse particle velocity V_B can be obtained from the measurements of the transverse particle velocity V_D at the free surface of the target plate and by employing the theory of stress wave propagation in the elastic target plate. However, to obtain the transverse particle velocity V_C an elastic-plastic analysis of stress wave propagation in the flyer plate is required.

Once the interfacial slip velocity is known, the temperature rise as a function of depth from the flyer-target interface can be estimated by solving the following one-dimensional transient heat conduction equation by Carslaw and Jaeger:[29]

$$\frac{\partial^2 T}{\partial x^2} = \frac{1}{\gamma}\frac{\partial T}{\partial t}, \tag{4}$$

with initial condition

$$T(x = 0) = 0, \tag{5}$$

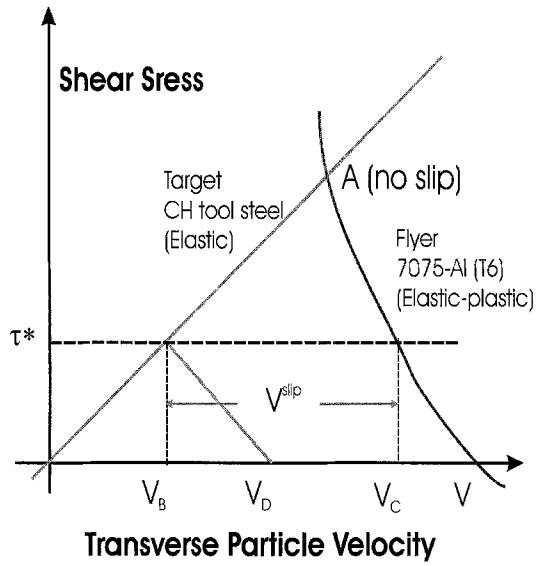

Fig. 3—Stress and particle velocity diagram for the elastic-plastic flyer impacting an elastic target plate

and boundary conditions

$$-k\frac{\partial T}{\partial x}(x=0,t)=\dot{q}(t), \tag{6}$$

$$T(x=\infty,t)=0. \tag{7}$$

In eqs (4)–(7), T is the temperature rise, t is time, k is the thermal conductivity, γ is the thermal diffusivity, $\dot{q}(t)$ is the heat source and x is the distance perpendicular to the interface. The temperature rise can be expressed as a function of time and position as

$$T(x,t)=\frac{1}{k}\int_0^t \dot{q}(\xi)\frac{\sqrt{\gamma}}{\sqrt{\pi(t-\xi)}}\exp\left(\frac{-x^2}{4\alpha(t-\xi)}\right)d\xi. \tag{8}$$

In order to calculate the temperature distribution in the tribo-pair materials, an estimate for the heat source $\dot{q}(t)$ is required. Using the experimentally measured friction stress τ, and slip velocity V^{slip}, the frictional power can be written as

$$\dot{q}_{7075-T6Al}(t)=\beta_1\tau(t)V^{slip}(t) \tag{9}$$

$$\dot{q}_{CH\,tool\text{-}steel}(t)=(1-\beta_1)\tau(t)V^{slip}(t). \tag{10}$$

In these equations, β_1 is the factor that governs the partitioning of heat in the two materials. The factor β_1 is estimated by equating the temperatures at the flyer-target interface to yield

$$\beta_1=\frac{k_1\sqrt{\alpha_2}}{k_1\sqrt{\alpha_2}+k_2\sqrt{\alpha_1}}. \tag{11}$$

In eq (11), k_1 and α_1 are the thermal conductivity and the thermal diffusivity of the aluminum alloy 7075-T6, respectively, and k_2 and α_2 are the thermal conductivity and the thermal diffusivity of the CH tool-steel. For the flyer/target material pair employed in the present investigation, the factor β_1 is approximately 0.607. Thus, 60.7% of the heat generated at the tribo-pair interface due to the frictional sliding goes into the aluminum alloy 7075-T6, while 39.3% is partitioned into the CH tool-steel plate.

Finite Element Simulations of the Elastic-plastic Pressure-shear Impact

One of the primary objectives for developing a finite-element based computational procedure for simulating the pressure-shear plate-impact experiments is to provide a methodology for obtaining reasonable estimates of interfacial slip-velocity from the measured free-surface particle velocity profiles. During the course of frictional sliding, a substantial amount of heat is generated due to friction at the contact surfaces and elastic-plastic interactions at the sliding interface. The rate at which heat is generated is obtained from the frictional power by using the computed slip-velocity history along with interfacial shear stress obtained by using eqs (4)–(11). Moreover, the rate of heat supply due to plastic work is estimated using $s=\beta\dot{W}^p$, where $\dot{W}^p$ is the plastic power per unit deformed volume and β is the Taylor-Quinney coefficient.[30] The frictional power and the computed plastic work are then used to obtain the temperature distribution in the flyer and target plates. Besides the temperature rise, the finite-element simulations provide fundamental information on the details of local elastic-plastic interactions at the sliding interface, including the formation and growth of molten aluminum layers and dynamic shearing resistance of the sliding interface as it passes through melt at ultra-high shearing rates.

The material is characterized as an isotropically hardening, and thermally softening elastic-viscoplastic von Mises solid. A combined power law and exponential plastic strain-rate relation,[31] that gives rise to enhanced strain-rate hardening at ultra-high strain rates,[32,33] is employed. Under high speed frictional sliding, it is anticipated that the reduction in material strength with increasing temperature will be the key mechanism that plays the dominant role in controlling the interfacial resistance. Under such conditions, a thermal softening Mises flow rule is found to be adequate. For the present simulations the particular form for the effective plastic strain rate $\dot{\varepsilon}^p$, that is chosen is based on the shear-stress shear-strain relationship over the strain rate range from 10^{-3} to 10^7 s^{-1}. The effective plastic strain rate $\dot{\bar{\varepsilon}}$, is taken to be of the form

$$\dot{\bar{\varepsilon}}=\frac{\dot{\varepsilon}_1\dot{\varepsilon}_2}{\dot{\varepsilon}_1+\dot{\varepsilon}_2}, \tag{12}$$

where

$$\dot{\varepsilon}_1=\dot{\varepsilon}_0\left[\frac{\bar{\sigma}}{g(\bar{\varepsilon},\theta)}\right]^m,\quad \dot{\varepsilon}_2=\dot{\varepsilon}_m\exp\left[-\frac{ag(\bar{\varepsilon},\theta)}{\bar{\sigma}}\right] \tag{13}$$

and

$$g(\bar{\varepsilon},T)=\sigma_0(1+\bar{\varepsilon}/\varepsilon_0)^N\left\{1-\beta[(\theta/\theta_0)^\xi-1]\right\}. \tag{14}$$

In eqs (13) and (14), $\bar{\varepsilon}=\int_0^t\dot{\bar{\varepsilon}}dt$ is the equivalent plastic strain, $\dot{\varepsilon}_m$ is a reference strain rate, m and a are the rate sensitivity parameters, respectively, σ_0 is a reference stress, ε_0 is a reference strain, N is the strain hardening exponent, θ_o is a reference temperature, and β and ξ are the thermal

softening parameters. The function $g(\bar{\varepsilon}, \theta)$ represents the stress-strain relation at a quasi-static strain rate of $\dot{\varepsilon}_0$ and at temperature θ. Equation (12) provides a smooth transition between the measured response $\dot{\bar{\varepsilon}} = \dot{\bar{\varepsilon}}_1(\bar{\sigma}, \bar{\varepsilon}, \theta)$ at strain rates less than 10^3 s^{-1}, and the limiting behavior $\dot{\bar{\varepsilon}} = \dot{\bar{\varepsilon}}_2(\bar{\sigma}, \bar{\varepsilon}, \theta)$ at strain rates greater than, say, 10^5 s^{-1}. The material strain-rate hardening response and temperature dependence of flow stress for the flyer and the target plates are shown in Figs. 4(a), 4(b) and 4(c). The material parameters used in the model are given in Tables 2 and 3 for CH tool-steel and 7075-T6 Al, respectively. These material parameters are borrowed from Rule and Jones.[34]

At temperatures above the melt temperatures, the material is modeled as a purely Newtonian fluid for which the dependence of the stress on the stretching tensor is linear.[35] In this case the stress tensor simplifies to

$$\sigma = -\omega \frac{(1 - J + \alpha(T - T_o))}{J} \frac{E}{(1 - \nu)} \mathbf{I} + \mu \mathbf{D}, \qquad (15)$$

where ω is the stiffness parameter, J is the Jacobian of the deformation, equal to the determinant of the total deformation gradient tensor, α is the thermal conductivity, T is the temperature, E is the elastic modulus, ν is the Poisson's ratio and μ is the dynamic shear viscosity of the fluid.

Figure 5 shows the finite element mesh used in conducting the numerical simulations of the experiments. The finite element discretization is based on triangular elements arranged in *crossed-triangle* quadrilaterals, such that the displacements and temperature vary linearly over the triangular elements. Nagtegaal *et al.*[36] have shown that an element of this type can accommodate isochoric deformations. This is of significance since plastic strain is volume preserving, and the total deformation at large strain is nearly isochoric. Moreover, plane-strain conditions are assumed to prevail. This condition, along with periodic boundary conditions, allows the flyer and target plates to be modeled by using a single column of finite elements. In the vicinity of the frictional interface the elements have dimensions of 1 μm × 1.5 μm.

TABLE 2—MATERIAL PARAMETERS USED TO DESCRIBE THE MATERIAL MODEL FOR CARPENTER HAMPDEN STEEL

E = 202 GPa, σ_0 = 2758 MPa
m = 100.0, β = 4.5
c_p = 422 J/(KgK), $\alpha = 1.0 \times 10^{-5}$ 1/K
a = 10.0, $\dot{\varepsilon}_0 = 1.0 \times 10^{-4}$ s^{-1}
$\dot{\varepsilon}_m = 5.0 \times 10^8$ s^{-1}, ε_0 = 0.014
k = 42.4.0 W/m·K, T_0 = 293 K
ξ = 0.12, N = 0.1, ν = 0.3

TABLE 3—MATERIAL PARAMETERS USED TO DESCRIBE THE MODEL FOR 7075-T6 ALUMINUM

E = 71 GPa, σ_0 = 572 MPa
m = 100.0, β = 3.6
c_p = 960 J/(KgK), $\alpha = 2.2 \times 10^{-5}$ 1/K
a = 5.2, $\dot{\varepsilon}_0 = 1.0 \times 10^{-4}$ s^{-1}
$\dot{\varepsilon}_m = 5.0 \times 10^6$ s^{-1}, ε_0 = 0.01
k = 130.0 W/m·K, T_0 = 293 K
ξ = 0.32, N = 0.1, ν = 0.33

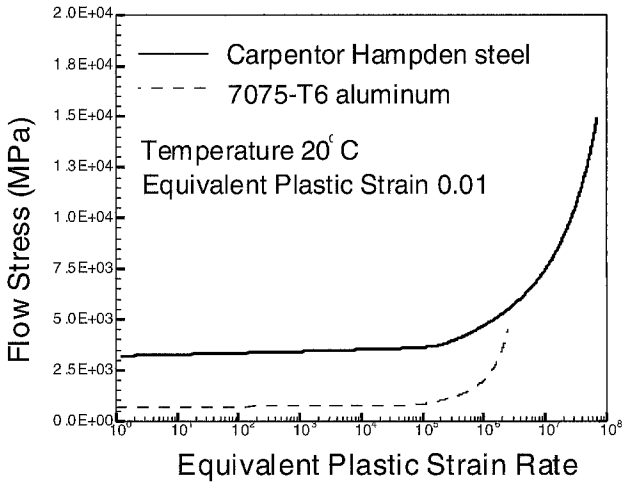

(a)

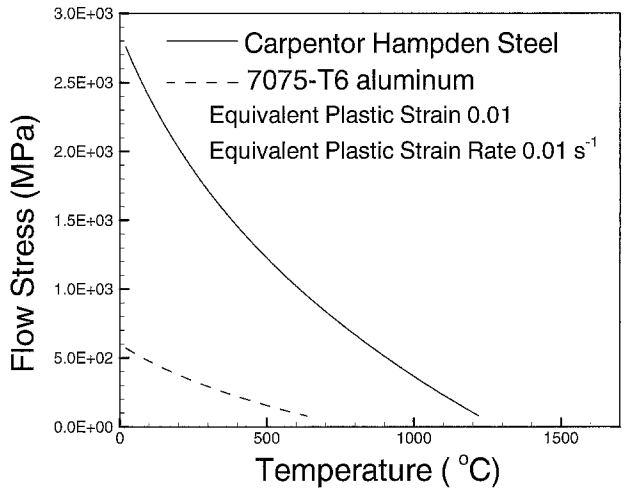

(b)

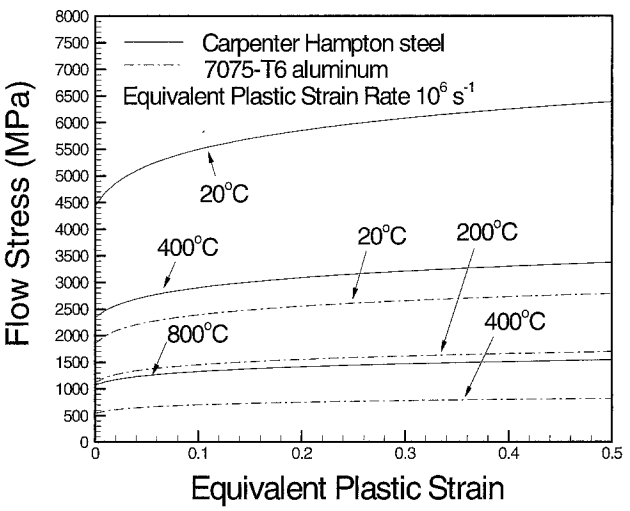

(c)

Fig. 4—(a) Flow stress versus plastic strain-rate dependence used in the viscoplastic model for the flyer and target plates, (b) flow stress versus temperature dependence used in the viscoplastic model for the flyer and target plates, and (c) flow stress versus equivalent plastic strain dependence for the flyer and target plates

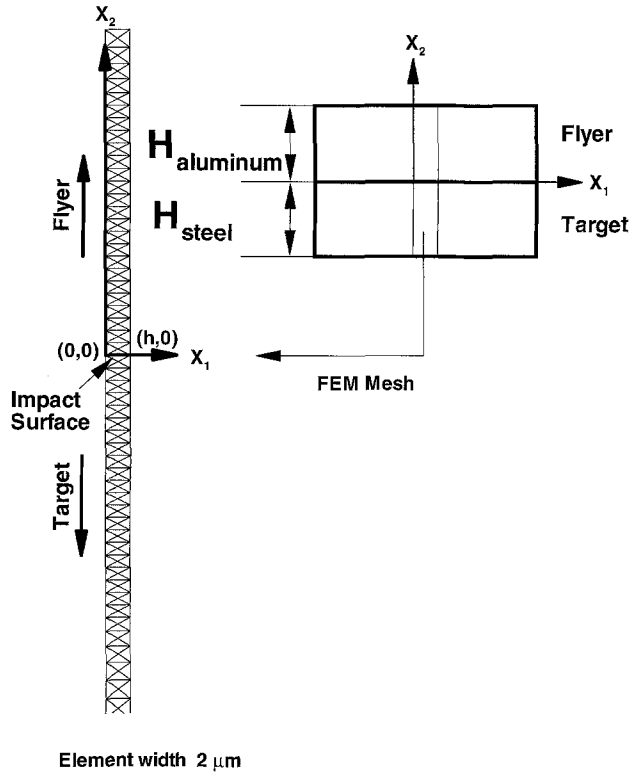

Fig. 5—Finite element mesh used in the simulation of the plate-impact pressure-shear experiments

Such small element size is necessary to resolve the sharp thermal and mechanical gradients in the vicinity of the sliding interface. The entire finite element mesh consists of 5863 quadrilateral elements with 35186 degrees of freedom.

With the origin of the coordinate system placed at the frictional, the boundary conditions for the particle velocities in 1 and the 2 directions, i.e., v_1 and v_2, the nodal forces in the 1 and 2 directions, i.e., f_1 and f_2, and temperature T can be can be written as

$$v_1(x_1 = 0, x_2, t) = v_1(x_1 = h, x_2, t) \quad (16)$$

$$v_2(x_1 = 0, x_2, t) = v_2(x_1 = h, x_2, t) \quad (17)$$

$$f_1(x_1 = 0, x_2, t) = f_1(x_1 = h, x_2, t) \quad (18)$$

$$f_2(x_1 = 0, x_2, t) = f_2(x_1 = h, x_2, t) \quad (19)$$

$$T(x_1 = 0, x_2, t) = T(x_1 = h, x_2, t). \quad (20)$$

In eqs (16)–(20), $-H_{steel} \leq x_2 \leq H_{aluminum}$
The initial conditions are

$$v_1(x_1, 0 \leq x_2 \leq H_{Aluminum}, t = 0) = V \cos\theta \quad (21)$$

$$v_2(x_1, 0 \leq x_2 \leq H_{Aluminum}, t = 0) = V \sin\theta \quad (22)$$

$$v_1(x_1, -H_{steel} \leq x_2 \leq 0, t = 0) = 0 \quad (23)$$

$$v_2(x_1, -H_{steel} \leq x_2 \leq 0, t = 0) = 0 \quad (24)$$

$$T(x_1, x_2, t = 0) = T_o. \quad (25)$$

In eq (25), T_o is the room temperature. Besides these boundary and initial conditions, contact-impact boundary conditions are applied on all flyer and target nodes at ($x_1 = 0, 0 \leq x_2 \leq h$), i.e., the impact surfaces.

Experimental Results and Discussion

Using the pressure-shear plate-impact experimental configuration, a series of experiments was conducted to investigate the dynamic shearing resistance of molten 7075-T6 Al alloy. Table 4 summarizes the experiments conducted in the present study. In all experiments 7075-T6 Al alloy was used as the flyer plate and the CH tool-steel was used as the target. The skew angle θ was kept constant at 35°. In order to promote high slip speeds the surface roughness of the flyer and target plates was kept relatively smooth. Moreover, the state of stress at the flyer-target interface was varied by changing the impact speed from 171 to 217 m/s.

The experimental results for SHOT 9906 are shown in Figs. 6 to 11. Figure 6 shows the normal and transverse particle velocity history recorded at the rear surface of the target plate by laser interferometry. The abscissa represents the time after impact. The compressive longitudinal wave arrives at the rear surface of the target plate at approximately 1620 ns. Upon arrival of the longitudinal wave, the normal component of the particle velocity jumps to approximately 98 m/s. Since a thick target plate was used in this particular experiment the normal pressure remains constant for the entire duration of the experiment. This can also be inferred from the near constant level of the measured normal particle velocity. The first arrival of shear wave at the free surface of the target plate occurs at approximately 2930 ns. This later arrival of the shear wave is consistent with the difference in longitudinal and the shear wave speeds in CH tool-steel. Upon arrival of the shear wave the transverse component of the particle velocity jumps to 18.2 m/s and then decreases gradually to a level of approximately 8 m/s during the experiment.

Figure 7 shows the history of the normal pressure, friction stress and interfacial slip velocity as a function of time for Shot 9906. The normal and transverse components of the interfacial tractions are obtained from the measured normal and transverse particle velocity profiles depicted in Fig. 6. The normal pressure remains constant at 2.24 GPa for the entire duration of the experiment. The interfacial shear stress jumps to 230 MPa at impact and then gradually decreases to a level of approximately 90 MPa. The dashed line corresponds to interfacial slip velocity obtained by using the measured interfacial shear stress and 1-D elastic wave theory, while the solid line represents the prediction based on the contact-impact thermo-elastic-plastic FEM analysis. Based on the 1-D elastic wave theory a monotonically increasing interfacial slip-speed ranging from 90 to 110 m/s is predicted. However, due to the extreme heat generated at the sliding interface, the interfacial temperature approaches the melt temperature of the aluminum alloy, leading to a no-slip condition at the molten-aluminum/CH steel interface. This occurs at approximately 1 μs, and is depicted in Fig. 7 as a precipitous fall in the slip velocity (represented by the solid line) from approximately 100 m/s to zero. The stick condition is followed by dynamic shearing of the molten Al layer sandwiched between the aluminum alloy and CH tool-steel plates.

Figure 8 shows the evolution of temperature at various depths in the aluminum alloy flyer-plate during the

TABLE 4—SUMMARY OF PLATE IMPACT PRESSURE-SHEAR EXPERIMENTS CONDUCTED IN THE PRESENT STUDY

SHOT #	Skew Angle θ, deg	Impact Velocity V m/s	Normal Stress σ_1, GPa	Roughness of 7075-T6 Al Alloy (Flyer) μm	Roughness of Carpenter Hampden Tool-steel (Target) μm
MO9904	35	171	1.762	0.11	0.01
MO9905	35	193	1.987	0.09	0.02
MO9906	35	217	2.242	0.07	0.02

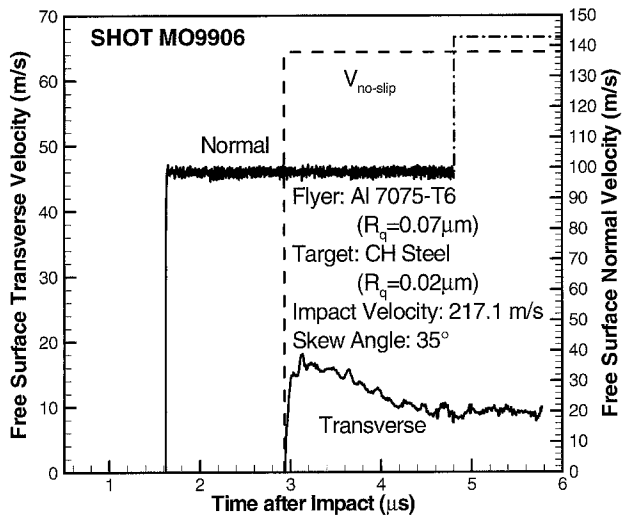

Fig. 6—Normal and transverse particle velocity history at the rear surface of the target plate

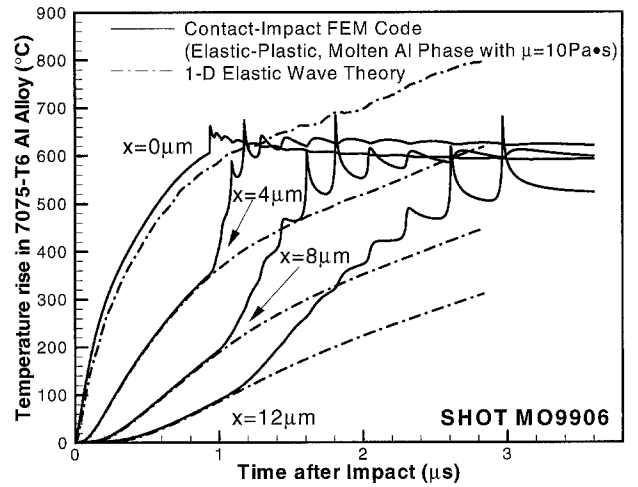

Fig. 8—Temperature profile in the aluminum alloy flyer-plate in the region near the sliding interface for Shot 9906. Note that fully melt interfacial temperatures are achieved at various depths in the aluminum alloy flyer plate

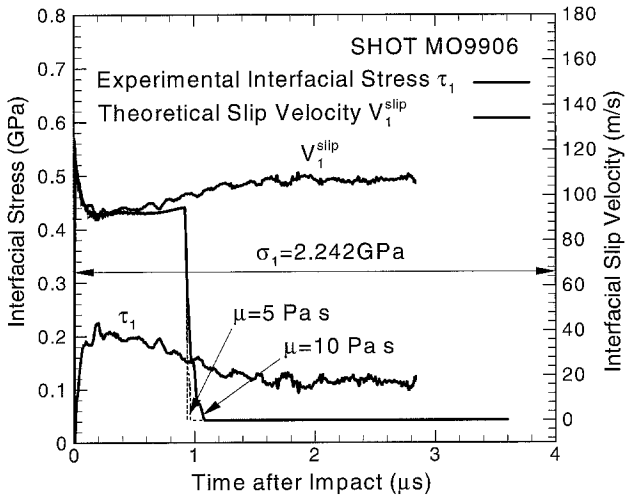

Fig. 7—History of the applied normal stress, friction stress and the slip velocity for Shot MO9906

high-speed slip process. The dashed curves represent the temperature profiles based on estimates of frictional power obtained from the measured friction stress and estimates of slip velocity based one-dimensional elastic-wave theory. The solid lines represent the corresponding temperature profiles as predicted by the thermo-elastic-plastic finite element simulations of the experiment. The diffusive nature of the solution to eq (8) is clearly evident from the sharp decay in bulk temperatures, along with a suppression of high frequency content in the temperature profiles with increasing depth from the frictional interface. The temperature profiles based of elastic-plastic finite element simulations and those predicted by the elastic-wave theory are in good agreement up to approximately 1 μs. This is consistent with the limited plasticity occurring during the early part of the slip process. However, after approximately 1 μs the increase in thermal stresses introduces significant deviatoric stresses to initiate localized plastic flow in the vicinity of the sliding interface. This results in a substantial increase in thermal heat generation due to plastic work. This is reflected in Fig. 8 for temperature profiles at small distances from the sliding interface by almost a vertical rise in interfacial temperature to the fully melt state.

Figure 9 shows the results of finite element simulations detailing the transition of the aluminum alloy from the solid to the molten phase. The solid line corresponds to the effective stress obtained by treating the molten aluminum as a perfectly viscous Newtonian fluid with a dynamic viscosity of 10 Pa-s, while the dashed line corresponds to simulations by assuming a dynamic viscosity of 5 Pa-s. For the case of dynamic viscosity of 10 Pa-s, during the early part of the transition from solid to molten phase, the computed shearing resistance is in excess of the measured shearing resistance. However, at later times the computed and the measured profiles are in much better agreement. With a 5 Pa-s dynamic

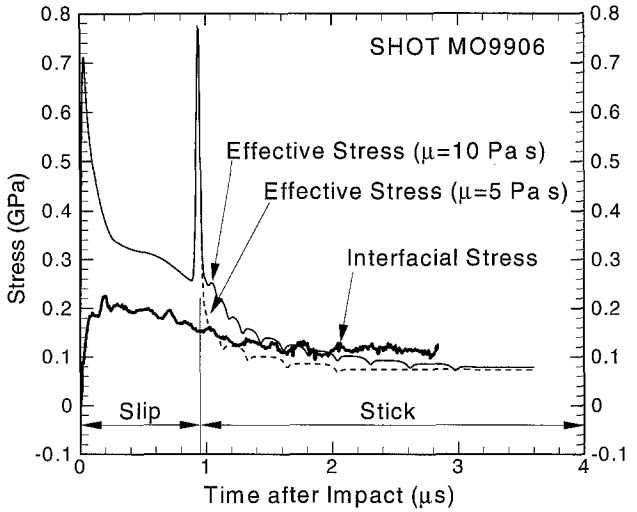

Fig. 9—Predictions based on finite element simulations of Shot MO9906 for the evolution of effective-stress for dynamic viscosities of 10 and 5 Pa-s

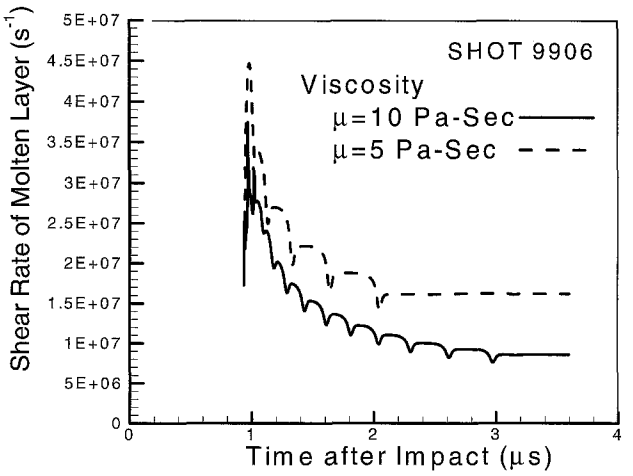

Fig. 10—Dynamic shearing-rate in the molten aluminum layer for Shot MO9906. Simulations are presented for dynamic viscosity corresponding to 10 and 5 Pa-s

viscosity the two curves are in much better agreement during the early part of the transition. It is to be noted here that the measured free surface transverse particle velocity at the rear surface of the target plate does not show any clear indication for the occurrence of the phase change. The authors believe that a clear indication of phase change would be present in the measured transverse component of the particle velocity if, during an experiment designed to measure the shearing resistance to plastic flow of a metal, there is a sudden change in phase from solid to melt during the deformation process. However, in the present experiments, prior to the transition in solid to melt phase, the transverse component of the particle velocity represents the resistance to frictional slip at the tribpair interface. This level of shear stress is already a fraction of the shearing strength of the metals representing the tribopair and thus does not show up as an abrupt change in the shearing resistance upon transition to melt conditions. Also, at early times during the transition process, the molten metal film is very thin and leads to mixed lubrication conditions at the flyer-target interface which includes both shearing of the molten film along with asperity to asperity contact. This situation again precludes any abrupt changes in the measured shear stress during the transition phase.

However, since under the fully-melt conditions the interfacial resistance is primarily due to dynamic viscosity of the molten metal layer, the measured limiting stress provides reasonable estimates of the shearing resistance of molten aluminum under high hydrostatic pressures and plastic shearing rates in excess of 10^7/s. It is interesting to note the relatively high level of shearing resistance of molten Al (approximately 100 MPa) under the experimental conditions of the present experiments. Efforts are in progress to explore formulations for dynamic viscosity, which can include pressure, temperature and rate dependence in order to better describe the observed shearing resistance of molten metals under conditions of the present experiments.

Figure 10 shows the growth kinetics of the molten aluminum layer as a function of the impact velocity. Simulations are presented for two different dynamic viscosity models corresponding to 10 Pa-s and 5 Pa-s. For 10 Pa-s, estimates for the thickness of molten aluminum are shown for the all the experiments conducted in the present investigation. However, for the case of dynamic viscosity of 5 Pa-s the thickness of the molten layer is shown only for Shot 9906. The depth of the molten layer, for a particular impact velocity, increases parabolically with time. The growth rate is highest at early times and decreases with growth of the molten layer thickness. Also, as expected, the thickness of the molten layer increases with an increase in impact velocity. It is interesting to note that the growth of molten layer is considerably less for the 5 Pa-s viscosity. This is due to the lower stress-power generated during shearing of the molten layer with 5 Pa-s viscosity as compared to the molten layer with a 10 Pa-s viscosity.

Figure 11 shows the shearing rates in the molten aluminum alloy layer as a function of time for Shot MO9906. Consistent with the growth of the molten aluminum layer, the dynamic shearing rate is highest immediately following the solid to melt transition and decreases thereafter with increasing molten layer thickness. Moreover, as also expected, the dynamic shearing rate obtained with the 5 Pa-s viscosity model is higher than that calculated with the 10 Pa-s dynamic viscosity model.

Figure 12 shows a plot for the dynamic shearing resistance of the confined molten 7075-T6 aluminum film as a function of normal pressure. It can be seen that the dynamic shearing resistance varies approximately linearly over the range of normal pressures employed in the present investigation, i.e., 0.5 to 2.5 GPa. It must be noted that these levels of dynamic shearing resistance correspond to dynamic viscosity in the range of approximately 5–10 Pa-s. These values of dynamic viscosity are in sharp contrast to the dynamic viscosity levels for molten aluminum reported by Mineev and Mineev[20] which were in the range of $2 - 4 \times 10^3$ Pa-s. One possible reason for this could be that, even though the dynamic shearing rates obtained in the present plate-impact pressure-shear experiments are similar to those obtained in Mineev and Mineev,[20] the normal pressures are very different. They range from 35–250 GPa, which is one to two orders of

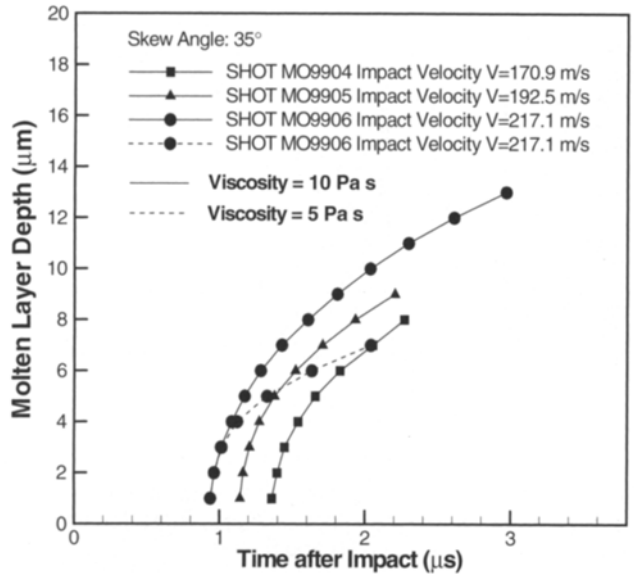

Fig. 11—Kinetics and growth of interfacial molten metal layers in aluminum alloy as a function of time for various impact velocities. For the highest impact velocity, i.e., 217 m/s simulations, based on dynamic viscosity of 10 and 5 Pa-s are presented

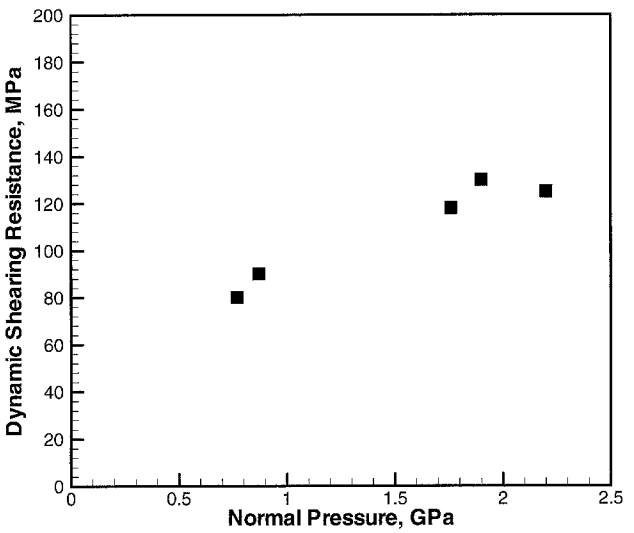

Fig. 12—Dynamic shearing resistance of the confined molten aluminum layer as a function of the applied normal pressure

magnitude higher than that obtained in the present plate-impact experiments.

Figure 13 shows a scanning electron micrograph depicting the frictional interface for Shot MO9906. Molten aluminum can be clearly seen smeared on the sliding surface. Along with the smeared molten metal there is a strong evidence of several subsurface cracks formed during the high-speed slip process.

Conclusions

In the present study a plate impact pressure-shear friction experiment is developed to study dynamic shearing resistance

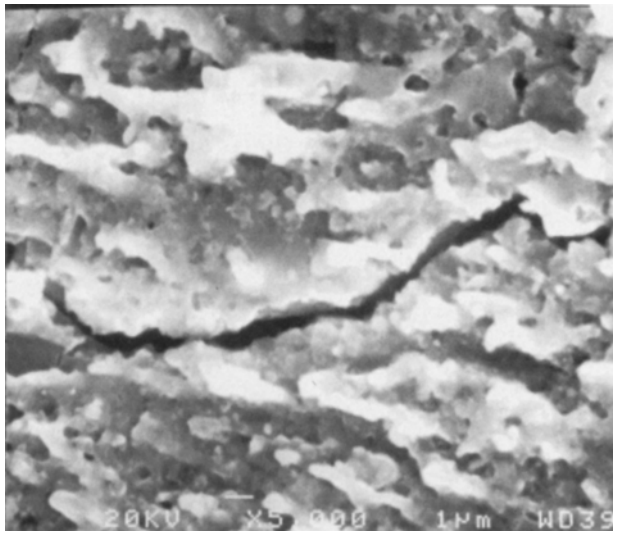

Fig. 13—A magnified view of the sliding surface for Shot MO9906. Molten metal is observed to be smeared on the sliding surface of the aluminum flyer plate

of molten metal films at high normal pressures and very high shearing rates. The results of the study indicate that molten Al films deformed at normal pressures of 1–2 GPa and dynamic shearing rates of 10^7 $1/s^{-1}$ maintain a shearing resistance as high as 100 MPa. These levels of dynamic shearing resistance correspond to a dynamic viscosity of 5–10 Pa-s. However, these values are significantly lower than those obtained by Mineev and Mineev,[20] which were in the range of $2-4\times10^3$ Pa-s at pressures of 35 to 250 GPa.

Acknowledgments

The authors would like to acknowledge the support of the Surface Science and Tribology program at the National Science Foundation for supporting this research.

References

1. Giovanola, J., Proceedings on Impact Loading and Dynamic Behavior of Materials, Bremen, Federal Republic of Germany (1987).

2. Marchand, A. and Duffy, J., "An Experimental Study of the Formation Process of Adiabatic Shear-bands in a Structural Steel," Journal of the Mechanics and Physics of Solids, **36** *(3), 251–283 (1988).*

3. Zhender, A.T. and Rosakis, A.J., "On the Temperature Distribution in the Vicinity of Dynamically Propagating Cracks in 4340VAR Steel: Experimental Measurements Using High Speed Infra-red Detectors," Journal of the Mechanics and Physics of Solids, **39**, *385–415 (1991).*

4. Zhou, M., Ravichandran, G., and Rosakis, A.J., "Dynamically Propagating Shear Bands in Impact-loaded Prenotched Plates-I: Experimental Investigations of Temperature Signatures and Propagation Speeds," Journal of the Mechanics and Physics of Solids, **44** *(6), 981–1006 (1996).*

5. Kolsky, H., "An Investigation of Mechanical Properties of Materials at Very High Rates of Loading," Proceedings Physical Society of London, **B-62**, *676–700 (1949).*

6. Lindholm, U.S., "Some Experiments with the Split Hopkinson Pressure Bar," Journal of the Mechanics and Physics of Solids, **12**, *317–335 (1964).*

7. Green, S.J., Maiden, C.J., Babcock, S.G., and Schierloh, F.L., "The High Strain-rate Behavior of Face Centered Cubic Metals," Proceedings of the 4th Batelle Memorial Institute Materials Science Colloquin on Inelastic Behavior of Solids 1969, pp. 521–542 (1970).

8. Duffy, J., Cambell, J.D., and Hawley, R.H., "On the Use of a Torsional Split Hopkinson Bar to Study Rate Effects in 1100-0 Aluminum," Journal of Applied Mechanics, **38**, *83–91 (1971).*

9. Harding, J., Wood, E.D., and Cambell, J.D., "Tensile Testing of Materials at Impact Rates of Strain," Journal of Mechanical Engineering Science, **2**, 88–96 (1960).

10. Hauser, E.F., "Techniques for Measuring Stress-strain Relations at High Strain-rates," EXPERIMENTAL MECHANICS, **6**, 395–402 (1966).

11. Lindholm, U.S. and Yeakley, L.M., "High Strain-rate Testing: Tension and Compression," EXPERIMENTAL MECHANICS, **8**, 1–9 (1968).

12. Nicholas, T., "Tensile Testing of Materials at High Strain Rates of Strain," EXPERIMENTAL MECHANICS, **21**, 177–185 (1980).

13. Li, C.H., A Pressure-shear Experiment for Studying the Dynamic Response of Metals at Shear Rates of 10^5/s, Providence, RI, Brown University (1982).

14. Clifton, R.J. and Klopp, R.W., "Pressure Shear Plate Impact Testing," Metals Handbook: Mechanical Testing, ASM, Metals Park, OH, Vol. 8, pp. 230–239 (1985).

15. Frutschy, K.J. and Clifton, R.J., "High-temperature Pressure-shear Plate Impact Experiments on OFHC Copper," Journal of the Mechanics and Physics of Solids, **46** (10), 1723–1743 (1998).

16. Assay, J.R. and Hayes, D.B., "Shock Compression and Release Behavior Near Melt States in Aluminum," Journal of Applied Physics, **46** (11), 4789–4800 (1975).

17. Schmidt, R.M., Davies, F.W., Lempriere, B.M., and Holsapple, K.A., "Temperature Dependent Spall Threshold of Four Metal Alloys," Journal of the Mechanics and Physics of Solids, **39** (4), 375–385 (1978).

18. Holsapple, K.A. and Schmidt, R.M., "Theory and Experiments on Rapid Melting of Metals Including Alloy Effects," Journal of Applied Physics, **49** (11), 5493–5501 (1978).

19. Schmidt, R.M., "A Viscoelastic Wave Propagation Model for Tungsten at Near-melt Conditions (3000K)," Journal of Applied Physics, **50** (4), 2600–2606 (1979).

20. Mineev, V.N. and Mineev, A.V., "Viscosity of Metals Under Shock-loaded Conditions," Journal De Physique IV, **7** (Colloque C3), 583–585 (1997).

21. Irfan, M.A. and Prakash, V., Contact Temperatures During Sliding in Pressure Shear Impact. Proceedings, Society of Experimental Mechanics Conference, Bethel, CT, SEM, 173–182 (1994).

22. Irfan, M.A. and Prakash, V., "Time Resolved Friction During Dry Sliding of Metal on Metal," International Journal of Solids and Structures, **37**, 2859–2882 (2000).

23. Liou, N.-S., Okada, M., and Prakash, V., Time Resolved Sliding of Metal-on-metal at Elevated Temperatures. A. Jennings. Proceedings of the Great Lakes Civil Engineering Graduate Student Research Symposium, Cleveland, Case Western Reserve University, 98–137 (2000).

24. Prakash, V., "A Pressure-shear Plate Impact Experiment for Investigating Transient Friction," EXPERIMENTAL MECHANICS, **35** (4), 329–336 (1995).

25. Rajagopalan, S., Irfan, M.A., and Prakash, V., "Novel Experimental Techniques for Investigating Time Resolved High Speed Friction," Wear, **225–229**, 1222–1237 (1999).

26. Kim, K.S., Clifton, R.J., and Kumar, P., "A Combined Normal and Transverse Displacement Interferometer with an Application to Impact of Y-cut Quartz," Journal of Applied Physics, **48**, 4132–4139 (1977).

27. Prakash, V., "Time-resolved Friction with Applications to High Speed Machining: Experimental Observations," Tribology Transactions, **41** (2), 189–198 (1998).

28. Barker, L.M. and Hollenbach, R.E., "Shock-wave Studies of PMMA, Fused Silica, and Sapphire," Journal of Applied Physics, **41** (10), 4208–4225 (1970).

29. Carslaw, H.S. and Jaeger, J.C., Conduction of Heat in Solids, 2nd ed., Oxford University Press, Oxford (1986).

30. Kobayashi, S., Oh, S.I., and Altan, T., Metal Forming and Finite Element Method, Oxford University Press, Oxford (1989).

31. Clifton, R.J., "High Strain Rate Behavior of Metals," Applied Mechanics Reviews, **43** (5, Part II), S9–S22 (1990).

32. Campbell, J.D. and Ferguson, W.G., "The Temperature and Strain Rate Dependence of the Shear Strength of Mild Steel," Philosophical Magazine, **21**, 63–82 (1974).

33. Klopp, R.W., Clifton, R.J., and Shawki, T.G., "Pressure-shear Plate Impact and Dynamic Viscoplastic Response of Metals," Mechanics of Materials, **4** (3-4), 375–385 (1985).

34. Rule, W.K. and Jones, S.E., "A Revised Form for the Johnson-Cook Strength Model," International Journal of Impact Engineering, **21** (8), 609–624 (1998).

35. Zhou, M., Ravichandran, G., and Rosakis, A.J., "Dynamically Propagating Shear Bands in Impact-loaded Prenotched Plates-II. Numerical Simulations," Journal of the Mechanics and Physics of Solids, **44** (6), 1007–1032 (1996).

36. Nagtegaal, J.D. and DeJong, J.E., "Some Computational Aspects of Elastic-plastic Large Strain Analysis," International Journal for Numerical Methods in Engineering, **17**, 15–41 (1981).